Research article

NMR IN BIOMEDICINE

Received: 26 August 2012, Revised: 29 July 2013, Accepted: 18 August 2013, Published online in Wiley Online Library: 24 September 2013

(wileyonlinelibrary.com) DOI: 10.1002/nbm.3024

Hyperpolarized ^{13}C NMR studies of glucose metabolism in living breast cancer cell cultures

T. Harris[a,b], H. Degani[b] and L. Frydman[a]*

The recent development of dissolution dynamic nuclear polarization (DNP) gives NMR the sensitivity to follow metabolic processes in living systems with high temporal resolution. In this article, we apply dissolution DNP to study the metabolism of hyperpolarized U-^{13}C,^{2}H$_7$-glucose in living, perfused human breast cancer cells. Spectrally selective pulses were used to maximize the signal of the main product, lactate, whilst preserving the glucose polarization; in this way, both C_1-lactate and C_3-lactate could be observed with high temporal resolution. The production of lactate by T47D breast cancer cells can be characterized by Michaelis–Menten-like kinetics, with $K_m = 3.5 \pm 1.5$ mM and $V_{max} = 34 \pm 4$ fmol/cell/min. The high sensitivity of this method also allowed us to observe and quantify the glycolytic intermediates dihydroxyacetone phosphate and 3-phosphoglycerate. Even with the enhanced DNP signal, many other glycolytic intermediates could not be detected directly. Nevertheless, by applying saturation transfer methods, the glycolytic intermediates glucose-6-phosphate, fructose-6-phosphate, fructose-1,6-bisphosphate, glyceraldehyde-3-phosphate, phosphoenolpyruvate and pyruvate could be observed indirectly. This method shows great promise for the elucidation of the distinctive metabolism and metabolic control of cancer cells, suggesting multiple ways whereby hyperpolarized U-^{13}C,^{2}H$_7$-glucose NMR could aid in the diagnosis and characterization of cancer *in vivo*. **Copyright © 2013 John Wiley & Sons, Ltd.**

Keywords: glucose metabolism; breast cancer; glycolytic intermediates; Warburg effect; DNP-enhanced NMR

INTRODUCTION

Changes in the metabolism of glucose (Gluc) have long been recognized as a distinctive feature of cancer. Malignant cells are associated with both elevated rates of glycolysis as well as a shift to anaerobic glycolysis, even under aerobic conditions – a condition known as the Warburg effect (1–3). The study of this aberrant metabolism is important to gain a better understanding of malignant transformations (4), as well as to develop therapeutic treatments that specifically target cancer cells, whilst showing minimum toxicity in normal tissues (5). The value of imaging the altered metabolism of cancer at a molecular level has been demonstrated by the widespread use of ^{18}F-fluorodeoxyglucose positron emission tomography scans in cancer imaging (6,7). NMR techniques may also be particularly well suited for the non-invasive detection and characterization of such metabolic processes. The investigation of living systems – either perfused cancer cells or animals with tumor models – using stable isotopically labeled metabolites, is consequently a mainstream approach to follow metabolism in preclinical studies (8–12). The analysis of the NMR features thus observed allows the activities of different enzymes to be defined, aids in the understanding of the metabolic regulation of cancer and characterizes how this process is affected by therapeutic treatments (13–16). These non-invasive molecular-level measurements are limited, however, by the inherently low sensitivity of NMR to these markers. Specifically, reliance on very informative but spectroscopically weak heteronuclei, such as ^{13}C or ^{15}N, challenges the real-time nature of the studies. Moreover, even if willing to compromise by relying on prolonged signal averaging times, it is often difficult to detect intracellular glycolytic intermediates, whose concentrations are usually much lower than those of the initial precursors or final products. For these reasons, biochemical studies aimed at the investigation of metabolism with high sensitivity and/or temporal resolution generally rely on destructive methods. In such instances, cells are 'pulsed' with isotopically labeled substrates, lysed after a short time, and the amounts of labeled products in the ensuing extracts are measured by sensitive high-resolution NMR or mass spectrometry methods (14,16–19).

The recent development of dissolution dynamic nuclear polarization (DNP) promises to alleviate these constraints by enhancing single-scan liquid-state ^{13}C NMR signals by more than 10 000-fold (20). In order to achieve this enhanced liquid-state NMR signal, nuclear polarization is generated in the solid state by transferring electron polarization to the nuclei of a co-glassed stable radical by microwave irradiation in a $\geq$3.3-T magnetic field at ~1–1.5 K (21). The sample is then rapidly melted and transferred to a detection magnet for the spectroscopic or imaging

* *Correspondence to: L. Frydman, Department of Chemical Physics, Weizmann Institute of Science, Rehovot 76100, Israel. E-mail: lucio.frydman@weizmann.ac.il*

a *T. Harris, L. Frydman*
Department of Chemical Physics, Weizmann Institute of Science, Rehovot, Israel

b *T. Harris, H. Degani*
Department of Biological Regulation, Weizmann Institute of Science, Rehovot, Israel

Abbreviations used: *DHAP, dihydroxyacetone phosphate; DNP, dynamic nuclear polarization; F16P, fructose-1,6-bisphosphate; F6P, fructose-6-phosphate; GAP, glyceraldehyde-3-phosphate; Gluc, glucose; G6P, glucose-6-phosphate; Lac, lactate; NTP, nucleotide triphosphates; PBS, phosphate buffer saline solution; PEP, phosphoenolpyruvate; 2PG, 2-phosphoglycerate; 3PG, 3-phosphoglycerate; Pyr, pyruvate; SNR, signal-to-noise ratio; ST, saturation transfer; T_1/T_2, longitudinal/transverse spin relaxation time.*

measurement. After melting of the sample, the hyperpolarized nuclear spins will return to thermal equilibrium according to their longitudinal relaxation time constants T_1. Although this process can be fast, suitable cases can be found in which the targeted compounds manage to retain enhancements of several orders of magnitude in their spin alignment, leading to unprecedented sensitivities. The utility of this technique to observe non-invasively molecular metabolism in living systems has been explored and demonstrated in numerous recent studies. The administration of hyperpolarized metabolites with ^{13}C enrichment at slow-relaxing nuclear sites – particularly 1-^{13}C-pyruvate (1-^{13}C-Pyr) (22–24), 2-^{13}C-fructose (25), ^{13}C-bicarbonate (26) and 1-^{13}C-lactate (1-^{13}C-Lac) (27) – has accordingly been used to characterize the altered metabolism associated with glycolysis. The present work explores the potential of DNP-enhanced methods for the study of glycolysis by observing directly the metabolism of hyperpolarized glucose (Gluc) in human breast cancer cell cultures. Gluc is a potentially relevant precursor for the identification of cancer metabolism; unlike the aforementioned metabolites, however, Gluc does not contain a non-protonated carbon group. The T_1 value of its protonated carbons is thus notoriously short [~1–2 s (28)] relative to the timescale required by *ex situ* DNP NMR – limited by the melting, transfer, injection and metabolic transformation of the target molecule. To deal with this obstacle, we used perdeuterated Gluc, increasing the T_1 value of its carbon atoms by approximately 10 times. The injection of hyperpolarized U-^{13}C,$^{2}H_7$-Gluc into a cell perfusion system (23) allowed us to monitor the metabolic features of living human breast cancer cells under controlled conditions using serial ^{13}C NMR acquisitions. The high sensitivity and scanning rate afforded by the ensuing set-up revealed Gluc → Lac production in cancer cells with high temporal resolution, as well as the direct observation of a number of glycolytic intermediates. Saturation transfer (ST) NMR methods also allowed us to detect indirectly glycolytic intermediates that were otherwise not observed directly. The ensuing ability to non-invasively follow the metabolism of Gluc in cancer cells, including the characterization of ~10 enzymatic steps and glycolytic intermediates, promises to become a valuable new tool to extract insights into the metabolic control of Gluc metabolism in cancers.

MATERIALS AND METHODS

Cell culture

Studies were performed using T47D clone 11 human breast cancer cells, kindly supplied by Professor I. Keydar (Tel-Aviv University, Tel-Aviv, Israel). The cells were cultured in RPMI-1640 medium supplemented with 10% fetal calf serum (Biological Industries, Beit-Haemek, Israel), 2 mM L-glutamine (CAS 56-89-5), 5 μg/L insulin and 0.1% combined antibiotics (Bio-Lab, Jerusalem, Israel). Cells were used in low passages. To implement the perfusion experiments, cells ($>3\times10^6$) were seeded on 0.5-mL Biosilon® polystyrene beads (160–300 μm; Nunc, Kamstrup, Denmark) placed in glass silanized vials. The vials were incubated for 3 h and periodically stirred every 30 min before transfer to bacteriological dishes. Medium was changed every second day as well as the day prior to the experiment. After 5–7 days of culture, cells were gathered into a 10-mm NMR test tube and connected to the perfusion system as described below. In each experiment, 20–80 million cells were observed in the coil volume.

Hyperpolarization

A 4 M self-glassing solution of U-^{13}C,$^{2}H_7$-D-Gluc (Cambridge Isotopes, Andover, MA, CAS 50-99-7) with 15 mM of the stable OX063 Trityl® radical (GE Healthcare Amersham, UK, CAS 213205-96-0) was prepared in D_2O. An aliquot of this sample, whose volume was tailored according to the desired final concentration, was inserted into the 3.35-T cold bore magnet of a Hypersense® dissolution DNP polarizer (Oxford Instruments, Tubney Woods, Abingdon, Oxfordshire, UK) and irradiated at ~93.96 GHz at 1.5 K to execute the DNP enhancement based on the solid effect (21). Solid-state ^{13}C polarization was monitored with low flip angle pulses during the course of the microwave irradiation. A characteristic buildup time of 53 ± 4 min was observed (Fig. 1, inset). After approximately 60 min of the DNP pumping process, the sample was dissolved in 5 mL phosphate buffer saline solution (PBS) heated to 180 °C and pressurized to 10 bar, and flushed into the perfusion–injection system. Following this dissolution and a transfer time of *ca*. 2 s to the detection magnet, a signal enhancement of approximately 13 000 was obtained, corresponding to polarization of ~13%. Twelve peaks corresponding to the α and β anomers of Gluc's six carbon sites were observed in the resulting ^{13}C NMR spectra (Fig. 1). The longitudinal relaxation times (T_1) of α-D-Gluc and β-D-Gluc were similar: C_1, C_2, C_3, C_4 and C_5 were all ~13.5 s and, for C_6, ~10.1 s, as measured on a 10 mM sample in PBS at ~35 °C.

Perfusion–injection system

The perfusion–injection system used in this work has been described previously in detail (23). In brief, cells were perfused with oxygenated medium in the NMR magnet at 36 ± 1 °C, and an additional inlet line allowed rapid injection of hyperpolarized solution. Two minutes prior to dissolution, perfusion was stopped and cells were washed with 2 mL of PBS through the hyperpolarized inlet line. Within 10 s of dissolution,

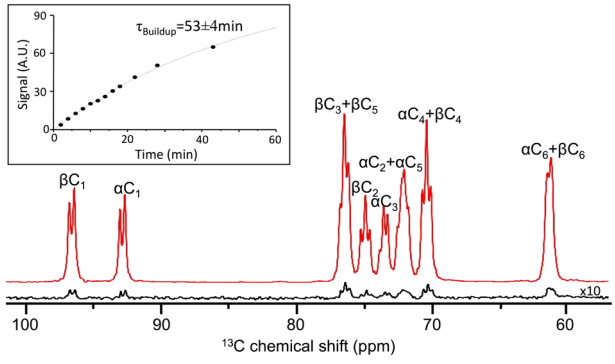

Figure 1. Dissolution dynamic nuclear polarization (DNP) of hyperpolarized U-^{13}C,$^{2}H_7$-glucose. Inset: build up of the solid-state ^{13}C polarization of 4 M U-^{13}C,$^{2}H_7$-glucose sample dissolved in D_2O containing 15 mM trityl radical when irradiated at 93.966 GHz at 1.5 K. Main figure: signal enhancement of ~13 000 times (~13% polarization) observed for a 6.7 mM solution of U-^{13}C,$^{2}H_7$-glucose hyperpolarized after 45 min of microwave irradiation (top trace, red) compared with a thermal equilibrium NMR spectrum (bottom trace, black). Both traces were measured at 125.74 MHz with ^{2}H decoupling, the hyperpolarized spectrum by a single scan with a 9° pulse, and the thermal equilibrium spectrum by 16 scans acquired with 45° pulses and a 60-s relaxation delay to ensure full return to thermal equilibrium.

3 mL of the hyperpolarized Gluc solution were manually injected into the cells. As this was performed with the perfusion stopped, there was no significant outflow of the metabolic products; the dense bead layout of the system also implied that no discernible turbulence accompanied the injection process. After each dissolution, the hyperpolarized inlet line was washed with 1 mL of PBS.

NMR measurements

NMR spectra were recorded on an 11.7-T, 63-mm bore magnet. Spectra were recorded using a Varian iNova® (Palo Alto, CA) spectrometer and a Bruker (Billerica, MA) 10-mm 'Quattro-Nucleus' (QNP®) probe. ^{31}P spectra were recorded at 202 MHz to monitor cell viability. The cell number was determined by analysis of these ^{31}P spectra, as it has been established that T47D cells contain 30 fmol nucleotide triphosphates (NTP)/cell (29) and therefore the cell number can be estimated from ^{31}P NMR as:

$$n_{\text{cells}} = \frac{(\text{NTP}/\text{Pi})\cdot[\text{Pi}]_{\text{Medium}}}{30\text{fmol NTP}/\text{cell}}\cdot V_{\text{ex}} \quad [1]$$

The fact that the ^{31}P and ^{13}C observations share the same coil volume and that the perfused system's volume always exceeded the coil region, allowed us to rely on these ^{31}P NMR data to further quantify the ^{13}C DNP results on a per cell basis.

^{13}C spectra were collected at 125 MHz after injection of the hyperpolarized Gluc solution. In order to preserve Gluc polarization, selective sinc pulses were created that applied 90° nutations in the carbonyl (170–220 ppm) and/or methyl (10–40 ppm) regions, whilst applying small flip angles (~1°) on the Gluc spectral region (60–100 ppm). For the indirect quantification of glycolytic intermediates, a train of selective pulses was applied at the chemical shift of the intermediate being sought before monitoring the C_1- and/or C_3-Lac spectra. (The parameters of the selective pulses are specified in the figure captions.) Chemical shift values of the intermediates were obtained from the literature (10,30) or measured in our laboratory (Table 1).

Kinetic model

A kinetic model for the quantification of the time-dependent signals arising from the transformation of hyperpolarized Gluc to Lac (Scheme 1) was developed. A complete derivation of the equations used in these fits can be found in APPENDIX A. In brief, on pulsing with a recycle time delay TR and with a low flip angle α_{Gluc} on the Gluc peaks and with a 90° pulse on the carbonyl and methyl peaks of Lac, the signals S_{Gluc} and S_{Lac} of hyperpolarized Gluc and Lac will vary as:

$$S_{\text{Gluc}}(t) = c\cdot\sin\ \alpha_{\text{Gluc}}\cdot[\text{Gluc}]_0\cdot P_{\text{Gluc}}(0)\cdot e^{-\frac{t}{T_{1,\text{Gluc}}}} \quad [2]$$

$$S_{\text{Lac}}(t,\text{TR}) = c\cdot\nu_{\text{Lac}}\cdot P_{\text{Gluc}}(0)\cdot e^{-\frac{t}{T_{1,\text{Gluc}}}}\cdot\left(\frac{e^{\Delta\rho\cdot\text{TR}}-1}{\Delta\rho}\right) \quad [3]$$

where $P_{\text{Gluc}}(0)$ is the Gluc polarization at time zero, $[\text{Gluc}]_0$ is its initial concentration, T_1 denotes the spin–lattice relaxation times, $\Delta\rho = \frac{1}{T_{1,\text{Gluc}}} - \frac{1}{T_{1,\text{Lac}}}$, c is a spectrometer-dependent constant whose value is unknown a priori, and ν_{Lac} is the rate of Lac generation.

Table 1. ^{13}C chemical shift values of relevant glycolytic metabolic intermediates. Each column indicates the glucose carbon from which a particular intermediate resonance derives; (*n*) indicates the intermediate's carbon numbering

Glycolytic metabolite	Originating ^{13}C Position in Glucose					
	1	2	3	4	5	6
αGluc[a]	92.4 (1)	71.5 (2)	73.0 (3)	69.8 (4)	71.7 (5)	60.4 (6)
βGluc[a]	96.2 (1)	74.4 (2)	76.0 (3)	69.8 (4)	75.9 (5)	60.5 (6)
αG6P[a]	92.6 (1)	72.8 (2)	72.5 (3)	69.3 (4)	71.3 (5)	62.5 (6)
βG6P[a]	96.5 (1)	74.5 (2)	75.4 (3)	69.3 (4)	75.6 (5)	62.6 (6)
αF6P[a]	63.0 (1)	105.5 (2)	81.0 (3)	76.2 (4)	81.4 (5)	64.4 (6)
βF6P[a]	62.7 (1)	102.6 (2)	75.7 (3)	74.6 (4)	80.8 (5)	64.8 (6)
αF16P[a]	65.3 (1)	105.6 (2)	82.0 (3)	76.3 (4)	81.2 (5)	64.4 (6)
βF16P[a]	65.9 (1)	102.0 (2)	76.0 (3)	74.3 (4)	79.6 (5)	64.8 (6)
DHAP[b]	65.4 (1)	212.6 (2)	67.7 (1)	67.7 (1)	212.6 (2)	65.4 (3)
GAP-Hyd[b]	62.4 (1)	74.8 (2)	90.7 (1)	90.7 (1)	74.8 (2)	62.4 (3)
3PG[c]	66.6 (1)	74.0 (2)	179.5 (1)	179.5 (1)	74.0 (2)	66.6 (3)
2PG[c]	64.6 (1)	77.4 (2)	178.9 (1)	178.9 (1)	77.4 (2)	64.6 (3)
PEP[a]	100.3 (1)	149.2 (2)	170.8 (1)	170.8 (1)	149.2 (2)	100.3 (3)
Pyr[b]	26.5 (1)	205.4 (2)	169.3 (1)	169.3 (1)	205.4 (2)	26.5 (3)
Lac[b]	20.1 (1)	69.6 (2)	183.5 (1)	183.5 (1)	69.6 (2)	20.1 (3)

DHAP, dihydroxyacetone phosphate; F16P, fructose-1,6-bisphosphate; F6P, fructose-6-phosphate; GAP, glyceraldehyde-3-phosphate; Gluc, glucose; G6P, glucose-6-phosphate; Lac, lactate; PEP, phosphoenolpyruvate; 2PG, 2-phosphoglycerate; 3PG, 3-phosphoglycerate; Pyr, pyruvate.

All chemical shifts measured on fully protonated compound are corrected by a factor of –0.36 ppm per C–^{2}H bond.

[a]Measured.

[b]From ref. (10).

[c]From ref. (30).

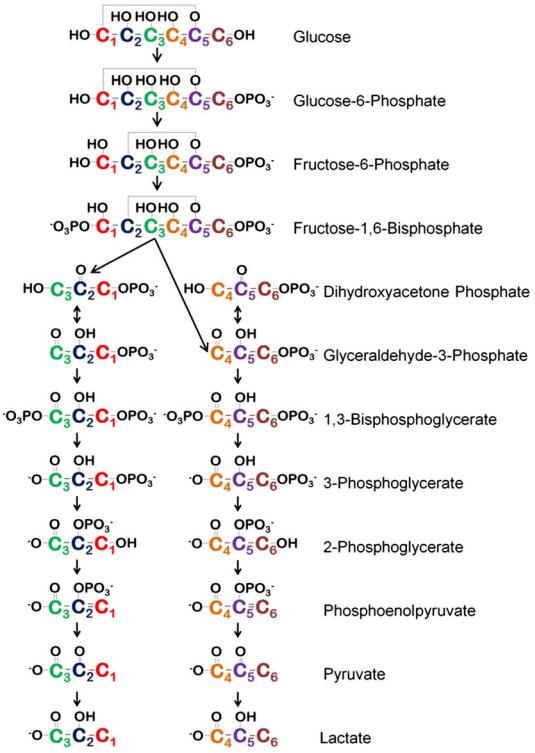

Scheme 1. Fate of ^{13}C atoms in the glycolytic pathway.

Normalizing the Lac peak by the Gluc signal at every time point yields:

$$R_{\mathrm{Lac}}(\mathrm{TR}) = \frac{S_{\mathrm{Lac}}(t,\mathrm{TR})}{S_{\mathrm{Gluc}}(t)} = \frac{\nu_{\mathrm{Lac}}}{\sin\alpha_{\mathrm{Gluc}}\cdot[\mathrm{Gluc}]_0}\cdot\left(\frac{e^{\Delta\rho\cdot\mathrm{TR}}-1}{\Delta\rho}\right) \quad [4]$$

This measurement is therefore independent of the instrument or degree of absolute Gluc initial polarization. A similar derivation can be performed for the signal of a hyperpolarized intermediate at steady state in the metabolic transformation Gluc $\xrightarrow{\nu_{\mathrm{Lac}}}$ Int $\xrightarrow{\nu_{\mathrm{Lac}}}$ Lac. To simplify this model, we assume T_1 homogeneity (i.e. $T_{1,\mathrm{Gluc}} = T_{1,\mathrm{Int}} = T_{1,\mathrm{Lac}}$) and negligible values for the rates of the back reaction. Then, $\nu_{\mathrm{Lac}} = f\cdot k_{\mathrm{Int}}\cdot[\mathrm{Int}]_{\mathrm{SS}}$, where $[\mathrm{Int}]_{\mathrm{SS}}$ denotes the intermediate's steady-state concentration and the factor $f = 1$ for three-carbon intermediates and $f = 2$ for six-carbon intermediates to account for the conversion of a six-carbon precursor into two identical three-carbon products (see APPENDIX B for a complete derivation of these relations). The signal of a hyperpolarized intermediate selectively pulsed at TR and normalized by $S_{\mathrm{Gluc}}(t)$ will then be:

$$R_{\mathrm{Int}}(\mathrm{TR}) = \frac{[\mathrm{Int}]_{\mathrm{SS}}}{\sin\alpha_{\mathrm{Gluc}}\cdot[\mathrm{Gluc}]_0}\cdot\left(1-e^{-\frac{\nu_{\mathrm{Lac}}}{f\cdot[\mathrm{Int}]_{\mathrm{SS}}}\cdot\mathrm{TR}}\right). \quad [5]$$

An important part of the measurements reported here concerns the signal reduction of the Gluc-normalized Lac signal as a result of pulsed saturation of a steady-state intermediate. This makes the Lac peak a reporter on the intermediate's concentration, leading to a type of pulsed ST measurement. The Gluc-normalized Lac signal on simultaneous intermediate pulsing will take the form (see APPENDIX B for complete derivations):

$$R_{\mathrm{Lac}}(\mathrm{TR}) = \frac{\nu_{\mathrm{Lac}}\cdot\mathrm{TR}}{\sin\alpha_{\mathrm{Gluc}}[\mathrm{Gluc}]_0} - \frac{[\mathrm{Int}]_{\mathrm{SS}}}{\sin\alpha_{\mathrm{Gluc}}[\mathrm{Gluc}]_0}\cdot\left(1-e^{-\frac{\nu_{\mathrm{Lac}}}{f\cdot[\mathrm{Int}]_{\mathrm{SS}}}\cdot\mathrm{TR}}\right) \quad [6]$$

It is also feasible and often convenient to pulse separately on the intermediate being saturated and on the Lac acting as reporter, i.e. to make $\mathrm{TR}_{\mathrm{Int}} \neq \mathrm{TR}_{\mathrm{Lac}}$. In such instances, the Gluc-normalized Lac signal will depend on both $\mathrm{TR}_{\mathrm{Int}}$ and $\mathrm{TR}_{\mathrm{Lac}}$ as:

$$R_{\mathrm{Lac}}(\mathrm{TR}_{\mathrm{Lac}},,\mathrm{TR}_{\mathrm{Int}}) = \frac{\nu_{\mathrm{Lac}}\cdot\mathrm{TR}_{\mathrm{Lac}}}{\sin\alpha_{\mathrm{Gluc}}[\mathrm{Gluc}]_0} - \frac{\mathrm{TR}_{\mathrm{Lac}}}{\mathrm{TR}_{\mathrm{Int}}}\cdot\frac{[\mathrm{Int}]_{\mathrm{SS}}}{\sin\alpha_{\mathrm{Gluc}}[\mathrm{Gluc}]_0}\cdot\left(1-e^{-\frac{\nu_{\mathrm{Lac}}}{f\cdot[\mathrm{Int}]_{\mathrm{SS}}}\cdot\mathrm{TRInt}}\right) \quad [7]$$

To improve the precision of such measurements, the ratio of the Gluc-normalized Lac signal in the presence and absence of intermediate pulsing can be derived:

$$Q_{\mathrm{Lac}}(\mathrm{TR}_{\mathrm{Int}}) = 1 - \frac{[\mathrm{Int}]_{\mathrm{SS}}}{\mathrm{TR}_{\mathrm{Int}}\cdot\nu_{\mathrm{Lac}}}\cdot\left(1-e^{-\frac{\nu_{\mathrm{Lac}}}{f\cdot[\mathrm{Int}]_{\mathrm{SS}}}\cdot\mathrm{TRInt}}\right) \quad [8]$$

Data analysis

The spectra arising from the hyperpolarized metabolites were obtained by Fourier transform of the time-domain signal – preceded by zero filling to 10 k points and exponential apodization with a 10–40-Hz Lorentzian lineshape – using custom-written routines (Matlab®, The Mathworks Inc., Nantucket, OH, USA). The spectra were fitted by Lorentzian peaks using DMFIT [The ComBase Consortium (31)], and the integrals of the fitted peaks were calculated to implement the above-mentioned kinetic derivations. The noise levels on the line intensities of the peaks were determined from the standard deviation of the lineshape fits; these noise levels were then propagated to derive the uncertainties on the reported flux observables. The time course of the integrals was fitted to the kinetic model described above using custom-written Matlab routines.

RESULTS

Insight into Lac production

^{13}C spectra acquired approximately 25 s after the injection of 5 mM of hyperpolarized U-^{13}C,$^{2}H_7$-Gluc to perfused T47D cells clearly reveal the production of labeled Lac by the appearance of a doublet peak at 183.5 ppm (C_1-Lac, Fig. 2a). To characterize this conversion whilst preserving Gluc as a source of hyperpolarization, as well as to improve our sensitivity to detect the fast-relaxing C_3-methyl group of Lac, the spectral separation between all the intervening peaks was exploited by collecting spectra using a shaped pulse that applied a low flip angle pulse (~1°) in the Gluc region (60–100 ppm) and 90° pulses to Lac's carbonyl (160–220 ppm) and/or methyl (0–40 ppm) regions. The recycle time delay for the carbonyl region was set at 3.6 s, whereas, for the methyl region, TR was set at 1.2 s, in order to maximize sensitivity for the respective T_1 values, whilst maintaining high temporal resolution [to account for the different $\Delta\rho\cdot$TR

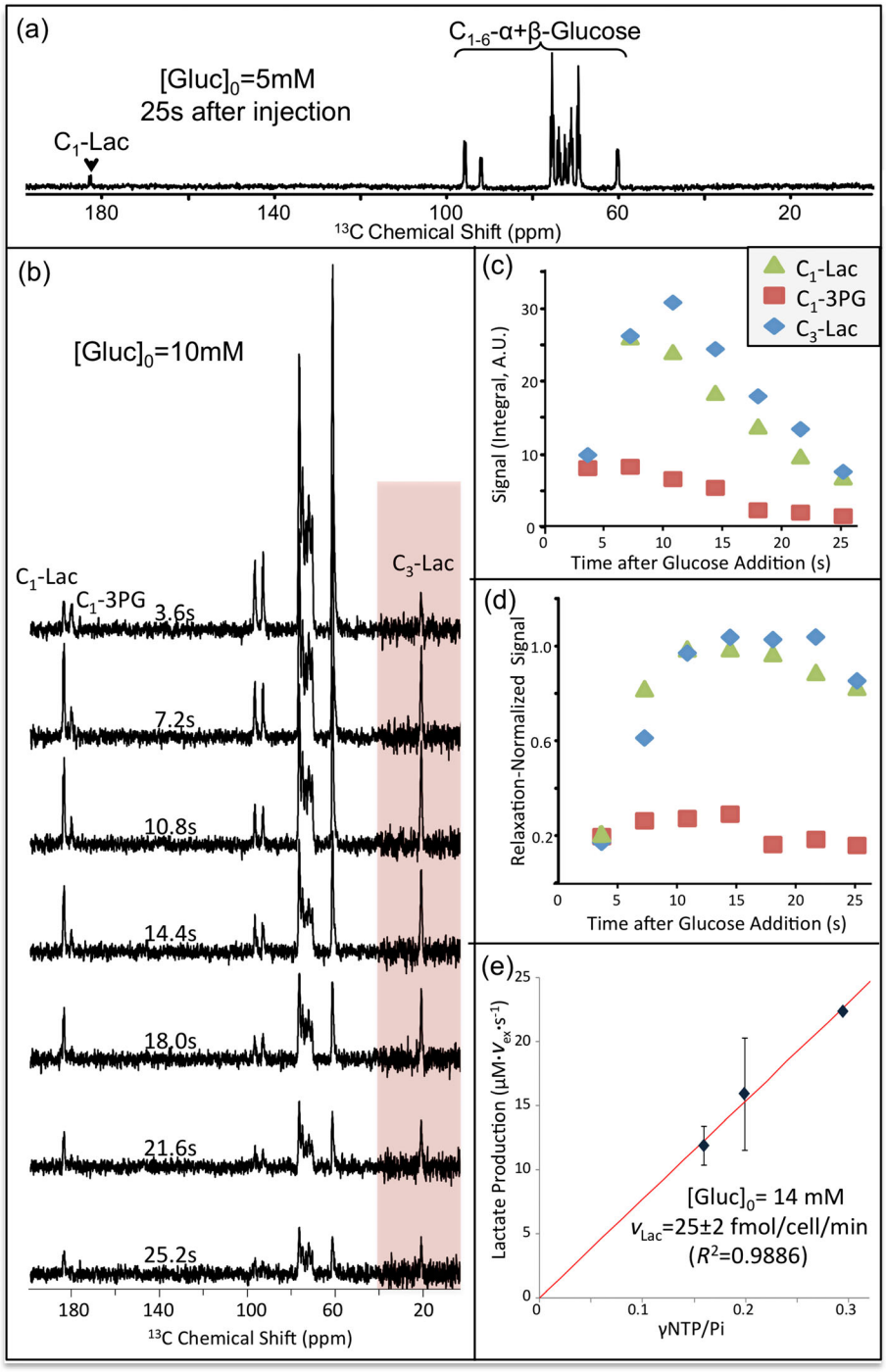

Figure 2. Characterization of the metabolism of hyperpolarized U-^{13}C,^{2}H$_7$-glucose in perfused T47D breast cancer cells. (a) ^{13}C spectra acquired 25 s after injection of 5 mM hyperpolarized glucose into perfused T47D cells using a hard, broad-band 90° pulse; in addition to glucose peaks (60–100 ppm), the C_1-lactate peak is observed at 183.5 ppm. (b) Series of ^{13}C spectra acquired after injection of 10 mM hyperpolarized glucose into perfused T47D cells. A shaped pulse was used applying a 90° excitation to the carbonyl region every 3.6 s, while the methyl region was pulsed with a 90° excitation every 1.2 s (shaded region; sum of three spectra shown). (c) Integrals of the C_1-lactate (▲), C_3-3PG (■) and C_3-lactate (♦) signals plotted as a function of time after the addition of hyperpolarized glucose. (d) As above, but after normalization by the glucose signal to correct for T_1 relaxation (C_1-lactate and C_1-3PG are corrected for C_2–C_5 glucose relaxation, whereas C_3-lactate is corrected by C_1 and C_6 glucose relaxation). (e) Correlation between the lactate production rates measured after the addition of 14 mM hyperpolarized glucose by ^{13}C NMR, and the γNTP/Pi ratio measured by ^{31}P NMR. ^{31}P spectra were acquired with a 45° pulse every 1 s, using a 0.5-s data sampling time. These rates were calculated from spectra acquired over 52 s following the injection of hyperpolarized glucose (see main text) with a selective pulse (sinc3, 65 ppm wide, centered at 188 ppm) applied at lactate's C1 resonance with TR = 20 s. The ratio of the peaks was divided by 2.15 to account for γNTP's shorter T_1 (i.e. incompletely relaxed Pi peak), calculated by comparison with a spectrum acquired with a long TR. The rate of lactate production for an initial glucose concentration of 14 mM was found to be 25 ± 2 fmol/cell/min (R^2 = 0.9886). Gluc, glucose; Lac, lactate; NTP, nucleotide triphosphates; 3PG, 3-phosphoglycerate; Pi, inorganic phosphate.

dependences; cf. Equation [3]]. Figure 2b, c shows the evolution of the Lac signal when followed in this manner, after the injection of 10 mM hyperpolarized Gluc into the cell culture. It can be seen that the relaxation-corrected hyperpolarized Lac signal reaches the constant value predicted by Equation [4] only at times longer than ~10 s after injection (Fig. 2d); the time lag needed to reach this constant level may be partially attributable to the time required for hyperpolarization to transfer through the metabolic intermediate pools, as discussed in the section on Indirect detection of 'invisible' intermediates.

Figure 2e shows that the rates of Lac production from Gluc correlate well with the γNTP/Pi ratio, reflecting the absolute number of cells involved. Using Equation [1], the per cell rate of Lac production from Gluc can be calculated. In order to further characterize this and other parameters of Gluc metabolism in T47D cells, the rate of Lac production was measured as a function of different initial Gluc concentrations. From this dependence (Fig. 3), it can be seen that the Gluc → Lac conversion process shows a saturation curve with Michaelis–Menten-like kinetics, yielding $V_{max} = 34 \pm 4$ fmol/cell/min and $K_m = 3.5 \pm 1.5$ mM ($R^2 = 0.9886$).

Direct detection and characterization of non-Lac intermediates

In addition to the Lac peaks at 20.8 and 183.5 ppm, injection of hyperpolarized Gluc into T47D cells revealed peaks at 212.5 and 179.9 ppm. Literature comparisons against metabolic chemical shifts suggest that these peaks should be assigned to C_2-dihydroxyacetone phosphate (C_2-DHAP) and C_1-3-phosphoglycerate (C_1-3PG), respectively. In order to better quantify these intermediates, the pulsing rate of the carbonyl region (160–220 ppm) was varied for a series of injections of 18 mM hyperpolarized Gluc. On modeling the ensuing 212.5- and 179.9-ppm signal behavior with Equation [3] (Fig. 4), concentrations of 0.31 ± 0.12 fmol/cell for DHAP and 0.18 ± 0.09 fmol/cell for 3PG were determined for this $[Gluc]_0 = 18$ mM case.

It is also worth noting that variation of the pulse rate on these glycolytic intermediates not only affects the latter's peak intensities, but also the Lac peak intensity. This can be clearly seen in the TR = 0.1 s case in Fig. 4a, where no Lac signal is observed. This can be explained by the fact that this end-product peak will only be observed if all of its precursors – starting from Gluc and continuing through all the glycolytic intermediates – remain hyperpolarized. It follows that, by modeling the decrease in Lac intensity caused by simultaneous pulsing of an intermediate [Equation [5]], the steady-state concentration of an intermediate can be determined indirectly. This will only hold true if the intermediate peak pulsed upon is transformed into a specific Lac peak; hence, the signal of C_1-Lac in Fig. 4 will reflect the concentration of 3PG, but not that of DHAP, as C_1-3PG is a precursor of C_1-Lac but C_2-DHAP is not (see Scheme 1). Using this relation, fits of the Lac peak observed on repeated pulsing in the carbonyl (160–220 ppm) region yielded an indirect quantification of the 3PG intermediate concentration of approximately 0.24 ± 0.06 fmol/cell (Fig. 4b, bottom plot). This value is similar to that obtained from the direct observation of 3PG (0.18 ± 0.09 fmol/cell), validating the ability of this indirect method to quantify an intermediate. It should be noted that this method of indirect quantification is parallel to ST experiments of the kind first proposed by Forsen and Hoffman (32).

Indirect detection of 'invisible' intermediates

Although the flux through all the intermediates of glycolysis is constant, differences in the enzymatic conversion rates imply that not all intermediates will reach the minimum concentration needed to enable their observation – even by hyperpolarized NMR. Nevertheless, given that both the initial and final metabolites of the glycolytic process (Gluc and Lac) are observable by DNP-enhanced ^{13}C NMR, these 'invisible' intermediates may be detected indirectly by rapidly pulsing – or even saturating – resonances corresponding to these low-concentration glycolytic species. However, the fast pulsing required to observe these low-concentration intermediates will reduce the signal-to-noise ratio (SNR) of the Lac signal. A valuable degree of freedom arising in such ST-type experiments involves the choice of different recycling delays to saturate the putative intermediate peak (TR_{Int}) from those used to observe the Lac peaks (TR_{Lac}). In this way, the intermediate can be pulsed at the fast rates needed to significantly depolarize the Lac signal, whereas the latter can be pulsed at a slower rate compatible with a higher SNR (see APPENDIX B for further details). The relationship between the Lac signal thus observed and the intermediate's nature is as summarized in Equation [7].

To control for variations between different injections in the Lac signal, as well as to compensate for inadvertent fluctuations in the polarization of Gluc arising from the saturation of the intermediate,

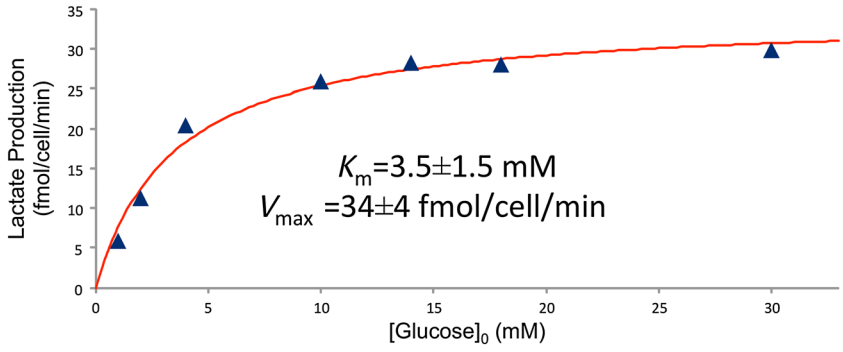

Figure 3. Rate of lactate production in T47D cells as a function of initial glucose concentration. The rates were calculated from spectra acquired 52 s after the injection of hyperpolarized glucose as described in the main text, with a selective pulse (sinc3, 65 ppm wide, centered at 188 ppm) applied at lactate's C1 resonance with TR = 20 s after injecting varying concentrations of hyperpolarized glucose ($R^2 = 0.9788$). Rates were found using Equation [4], with T_1 of C_1-lactate set as 17 s and T_1 of C_3- and C_4-glucose set at 13.5 s, as derived from *ad hoc* inversion recovery measurements. Fitting these data to the Michaelis–Menten rate equation, $v_{Lac} = \frac{V_{max} \cdot [Gluc]_0}{K_m + [Gluc]_0}$, yielded $K_m = 3.5 \pm 1.5$ mM and $V_{max} = 34 \pm 4$ fmol/cell/min ($R^2 = 0.9788$).

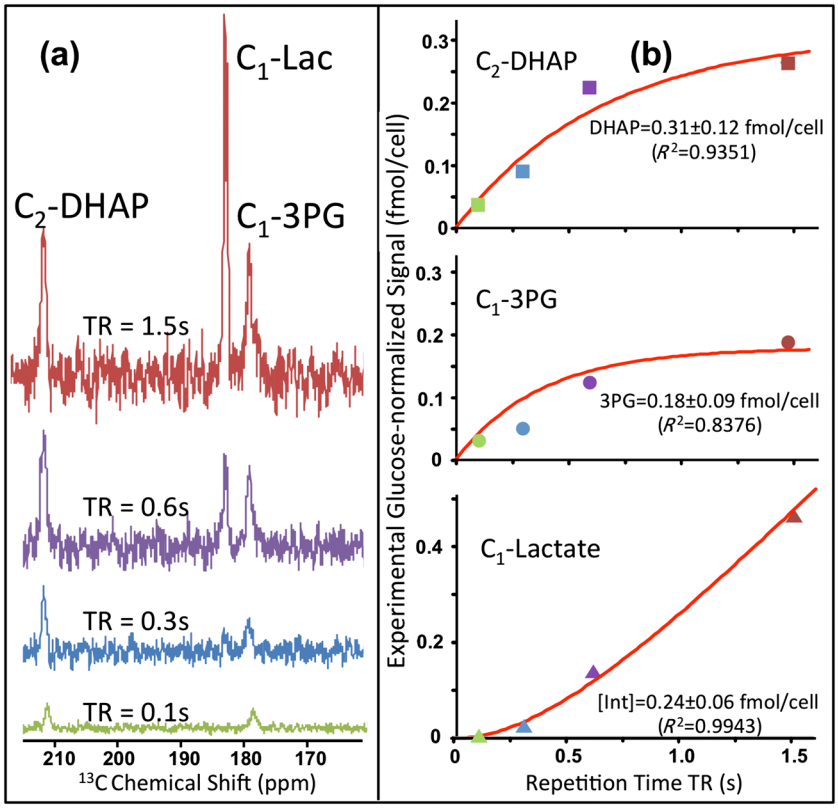

Figure 4. Characterization of the carbonyl region peaks observed on injection of hyperpolarized glucose. (a) Co-added ^{13}C NMR spectra acquired between 8 and 26 s after injection of 18 mM hyperpolarized U-^{13}C,^{2}H$_7$-glucose, collected for TR = 1.5, 0.6, 0.3 and 0.1 s. All spectra are normalized to the C_2–C_5 glucose signals. A selective 90° pulse was applied in the 160–220-ppm range. (b) Fitting of the C_2-DHAP (212.5 ppm) and C_1-3PG (179.9 ppm) hyperpolarized signals to Equation [5] and of the C_1-lactate signal (183.5 ppm) to Equation [6] when pulsing on the a priori known 3PG C_1 position. For all fits, the rate of lactate production was fixed at 28.5 fmol/cell/min (the value indicated in Fig. 3 for $[Gluc]_0 = 18$ mM). Points in these plots correspond to the intensities measured in the corresponding colored spectra, and lead to the indicated steady-state *in vivo* concentrations. DHAP, dihydroxyacetone phosphate; Lac, lactate; 3PG, 3-phosphoglycerate.

the Lac signal of a given experiment was evaluated in the presence and absence of pulsing of an intermediate, following its normalization by the Gluc resonance [Equation [8]]. The ability of this approach to observe and quantify glycolytic intermediates is demonstrated in Fig. 5. The top panel in this figure compares Lac's signal on pulsing in two different regions: 178.8–181.3 ppm, corresponding to the C_1 atoms of 3PG and 2-phosphoglycerate (2PG), and 175.5–178.0 ppm, a region expected to be free from any intermediates. The normalized, relaxation-corrected Lac signals of tests carried out for $TR_{Int} = 100$ ms and $TR_{Lac} = 2.4$ s (Fig. 5b) reveal that, on pulsing at 178.8–181.3 ppm, these signals decrease by ~70% compared with counterpart time points when intermediate pulsing was stopped, whereas no significant effects are seen on pulsing in the 175.5–178.0-ppm region.

Based on this validation, this indirect method was used to explore several other glycolytic intermediates. Using the known chemical shifts of the glycolytic intermediates, regions of radiofrequency pulsing were chosen that met the following criteria: (i) the intermediate's peak was a precursor of either the C_1- or C_3-Lac site; and (ii) the intermediate pulsing region did not overlap with its precursor Gluc peaks. In all cases, TR_{Lac} for the C_1 and/or C_3 peak was set to 2.4 s, whereas TR_{Int} for the region(s) in which the intermediate was pulsed upon was varied to maximize the sensitivity to the intermediate's concentration (by searching for the TRs that resulted in the most significant reduction in the signal of Lac). The resulting Q_{Lac} values – describing the Gluc-normalized quotient of the Lac signal with and without pulsing on the intermediates – are summarized in Table 2. In the simplest case, where only one intermediate that transforms to a given Lac site is pulsed upon, these will reflect directly the intermediate's concentration [Equation [8]]. A summary of the ensuing *Q*-derived results revealed the following:

- Pulsing on the expected site of C_3-Pyr (27.3 ppm) at $TR_{Int} = 40$ and 100 ms resulted in 44 ± 10% and 28 ± 6% reductions in the C_3-Lac signal, respectively.
- Pulsing on the hydrate peak of C_1-glyceraldehyde-3-phosphate (C_1-GAP) (the stable form for this molecule *in situ*) at 91.1 ppm with $TR_{Int} = 20$ ms resulted in a 23 ± 5% signal reduction in C_1-Lac.
- The peak of C_3-phosphoenolpyruvate (C_3-PEP) falls at 101.0 ppm, making it difficult to repetitively pulse this position without affecting the polarization of its C_1-β-Gluc precursor. However, as C_3-PEP originates from C_1 and C_6 of Gluc, presaturation of C_1-Gluc enabled us to monitor the effect more precisely (although at the cost of reducing by half the maximum SNR of the C_3-Lac signal): pulsing C_1 of Gluc at $TR_{Int} = 20$ ms yielded a 68 ± 4% signal reduction in the remaining C_3-Lac signal.
- When attempting to monitor glucose-6-phosphate (G6P), the only peak that was sufficiently well resolved from Gluc was C_6-G6P – a precursor of C_3-Lac. However, it was difficult to selectively pulse this peak, as it is separated by less than 0.1 ppm from the C_1 of fructose-6-phosphate (F6P), also a precursor of C_3-Lac. This problem was circumvented by

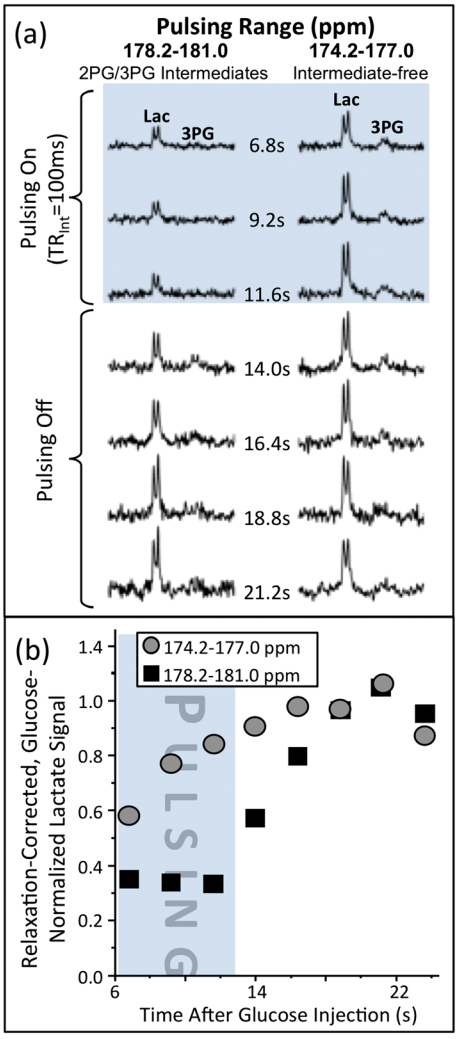

Figure 5. Indirect detection of glycolytic intermediates by observation of a concomitant decrease in the lactate signal. (a) Time evolution of the C_1-lactate NMR signal (normalized for T_1 relaxation) after injection of 10 mM hyperpolarized U-^{13}C,$^{2}H_7$-glucose and pulsing at TR_{Int} = 100 ms in the range 178.2–181.0 ppm (left column) and 174.2–177.0 ppm (right column). In both instances, 17.3-ms-long sinc pulses were used, and the saturation range is defined as the region for which Bloch-based simulations show a >80% excitation of the spin polarization. After 11.6 s, pulsing was stopped and the recovery of the lactate signal was observed. (b) Lactate's normalized, relaxation-corrected C_1 signal intensity as a function of time after injection of hyperpolarized glucose. Note that there is a certain time lag in both the buildup of hyperpolarized lactate when the intermediate is not pulsed upon (gray circles), as well as in the lactate saturation when implementing pulsing on an intermediate's peak (black squares). Both of these presumably reflect the finite turnover rates of the glucose → intermediate → lactate metabolic process. Because of this, the R_{Lac} and Q_{Lac} values (e.g. Table 2) were calculated using as reference the last spectral sets acquired before the intermediate's pulsing was stopped (in this case, data points at 11.6 s after the glucose injection). 2PG, 2-phosphoglycerate; 3PG, 3-phosphoglycerate.

exploiting the fact that C_6-G6P originates from C_6-Gluc, whereas C_1-F6P originates from C_1-Gluc. In order to observe only G6P, we presaturated C_1-Gluc and pulsed the 63–64-ppm region at TR_{Int} = 50 ms and 100 ms, yielding 82 ± 4% and 50 ± 6% reductions, respectively, in the remaining C_3-Lac signal.

- Conversely, to selectively observe F6P, C_6-Gluc in the 63–64-ppm region was presaturated by pulsing at TR_{Int} = 40 ms, yielding a 60 ± 6% reduction in the remaining C_3-Lac signal.

For several glycolytic intermediates, selective pulsing on a sole species is not possible because of extensive overlap. In such cases, the reduction in the Lac signal can no longer be described by Equation [8], and hence only qualitative conclusions can be derived. Examples of such instances include:

- The C_1 peaks of 3PG and 2PG are not well resolved; pulsing in their region results in 65 ± 3% and 79 ± 3% signal reductions of C_1-Lac for TR_{Int} = 100 and 50 ms, respectively.
- Pulsing the overlapping C_4 peaks of F6P and fructose-1,6-bisphosphate (F16P), together with saturation of C_3-Gluc at TR_{Int} = 100 ms, resulted in a 92 ± 10% reduction in the remaining C_1-Lac signal.
- Another interesting application of this approach arises on pulsing at the frequencies expected for the overlapping C_3 peaks of αF6P and αF16P. At TR_{Int} = 100 ms, this resulted in a 47 ± 2% reduction in the C_1-Lac signal, suggesting that αF6P and/or αF16P are abundant in T47D cells.

It should also be noted that, in these pulsed ST experiments, Lac's signal recovery is not immediate after the pulsing on an 'invisible' intermediate stops. This lag time reflects the time required for repolarization of the intermediate pools to Gluc-dictated polarization levels. This effect can be seen in Fig. 5a, which shows that, 2.4 s after pulsing on the 3PG + 2PG intermediate stops (at a post-injection time of 14 s), the Lac signal has only recovered by approximately 40%; by contrast, the 3PG peak exhibits full recovery much sooner. Similar recovery delays in the Lac signal can be seen for many other intermediates (Fig. 6a). An interesting trend can be noted in the sequential order of the intermediates along the glycolytic pathway, and the percentage of the Lac signal observed after a given polarization recovery delay (Fig. 6b).

DISCUSSION AND CONCLUSIONS

This study explored the metabolism of Gluc in living T47D human breast cancer cells using novel hyperpolarized ^{13}C NMR acquisition schemes. We have thus expanded the previous work of Meier *et al*., who observed the metabolism of hyperpolarized Gluc in yeast (33) and *Escherichia coli* cell suspensions (34,35), to the study adherent mammalian cancer cells. We were able to maximize the product signal whilst preserving the Gluc hyperpolarization by exploiting the ^{13}C T_1 lengthening afforded by extensive deuteration and the spectral separation between Gluc and its products, and by applying various frequency-selective excitation and saturation strategies. Only by combining the unique molecular insights available from chemical shifts, the non-invasiveness of *in situ* perfusion NMR, and the outstanding sensitivity provided by *ex situ* DNP, could the kind of information that has been described here become available.

From an NMR perspective, the pulsed ST methods described here showed great promise in improving the sensitivity of MR measurements to reaction intermediates whose concentrations are too low for direct detection - even after dissolution DNP. In addition to the four orders of magnitude improvement in sensitivity provided by the hyperpolarization, the ST experiments furnish an additional signal sensitivity, as only newly formed end-products are observed. These experiments are still sensitive to the sources of error present in thermal NMR ST, i.e. incomplete depletion of the intermediate, inadvertent depletion of the product, reactant or other intermediates that are not meant to be addressed, etc. However, the weight of these different

Table 2. Summary of saturation transfer experiments performed to characterize glycolytic intermediates, $[Gluc]_o = 10$ mM

Molecule	Intermediate site(s) pulsed	Selective pulse and saturation range[a]	Gluc site presat	Lac site obs	TR_{Int} (ms)	Q_{Lac}[b]	% recovered 2.4 s after intermediate pulsing stopped[b]	fmol/10^3 cells[b]	R^2[e]
G6P	C_6-α + β-G6P (62.5 + 62.6 ppm)	sinc3 (17.2 ms) 62.3–65.0 ppm	C_1	C_3	50	0.57 ± 0.01[d]	29 ± 4	34 ± 6	0.818
					100	0.70 ± 0.01[d]	7 ± 7	19 ± 2	
F6P	C_6-α + β-F6P (63.0 + 62.7 ppm)	sinc3 (15.9 ms) 62.2–65.1 ppm	C_6	C_3	40	0.70 ± 0.03[d]	44 ± 16	8 ± 2	
αF6P + αF16P	C_3-α-F6P + F16P (81.0 + 82.0 ppm)	sinc5 (11.4 ms) 76.8–83.7 ppm	–	C_1	100	0.53 ± 0.02	40 ± 7		
F6P + F16P	C_4-α + β-F6P + C_4-α + β-F16P (76.2 + 74.6 + 76.3 + 74.3 ppm)	sinc5 (11.4 ms) 71.8–78.7 ppm	C_3	C_1	100	0.54 ± 0.05[d]	16 ± 17		
GAP-Hyd	C_1-GAP-Hyd (90.7 ppm)	sinc3 (2.7 ms) 85.9–103.6 ppm	–	C_1	20	0.77 ± 0.05	49 ± 38	2 ± 1	
3PG + 2PG	C_1-3PG + C_1-2PG (179.5[c] + 178.9 ppm)	sinc3 (17.2 ms) 178.2–181.0 ppm	–	C_1	50	0.21 ± 0.03	39 ± 7	42 ± 8	0.994
					100	0.35 ± 0.03	34 ± 8	45 ± 5	
PEP	C_3-PEP (100.3 ppm)	sinc3 (2.7–ms) 85.9–103.6 ppm	C_1	C_3	20	0.32 ± 0.04	49 ± 11	10 ± 2	
Pyr	C_3-Pyr (26.5 ppm)	sinc3 (17.2 ms) 25.6–28.6 ppm	–	C_3	40	0.56 ± 0.05	78 ± 21	8 ± 5	0.691
					100	0.72 ± 0.06	13 ± 33	15 ± 3	

F16P, fructose-1,6-bisphosphate; F6P, fructose-6-phosphate; GAP, glyceraldehyde-3-phosphate; Gluc, glucose; G6P, glucose-6-phosphate; PEP, phosphoenolpyruvate; 2PG, 2-phosphoglycerate; 3PG, 3-phosphoglycerate; Pyr, pyruvate.

[a]Saturation region defined as regions with >80% excitation.

[b]Error calculated from uncertainty in integral derived by curve fitting.

[c]This is the chemical shift reported in the literature; however, this pH-sensitive chemical shift resonates at 179.9 ppm in our measurements.

[d]Corrected for saturation of 50% precursor glucose signal, assuming C_1/C_6 and C_3/C_4 contribute equally to C_3- and C_1-lactate signals, respectively.

[e]Calculated when fitting both results to Equation [8].

NMR IN BIOMEDICINE

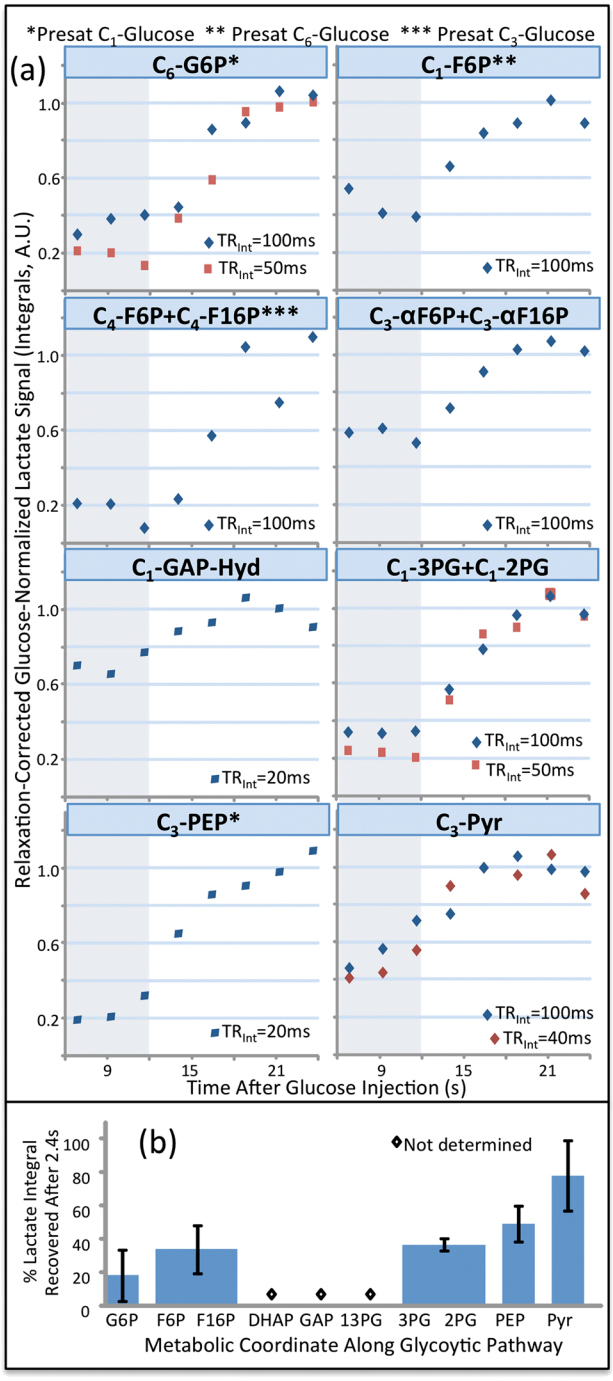

Figure 6. Response of lactate hyperpolarized signal to repetitive pulsing on selected glycolytic intermediates. (a) Relaxation-corrected, glucose-normalized lactate signal detected after injection of 10 mM hyperpolarized U-^{13}C,$^{2}H_7$-glucose, during (shaded areas) and after pulsing on a putative intermediate's region targeting the indicated resonances. When more than one species is indicated, it means that spectral overlap did not enable the resolution of the specified intermediate's peaks. Indicated in each plot is the TR at which the intermediate was pulsed upon with 90° sinc3 pulses, as described in Table 2. (b) Percentage of lactate polarization recovered 2.4 s after the intermediate's pulsing was stopped, plotted in the sequential order of the glycolytic pathway. Diamonds denote intermediates that were not measured or for which the measurement's uncertainty exceeded the confidence interval. DHAP, dihydroxyacetone phosphate; F16P, fructose-1,6-bisphosphate; F6P, fructose-6-phosphate; GAP, glyceraldehyde-3-phosphate; G6P, glucose-6-phosphate; PEP, phosphoenolpyruvate; 2PG, 2-phosphoglycerate; 3PG, 3-phosphoglycerate; 13PG, 1,3-phosphoglycerate; Pyr, pyruvate.

sources of errors is different in hyperpolarized than in thermal ST NMR. Inadvertent saturation of the product site, for example, should be less critical in hyperpolarized ST NMR, as the dynamic range of these experiments is wider (one is not relying on a small change sitting on top of a large peak, but rather on the appearance/disappearance of a newly formed product). Moreover, hyperpolarized ST should be more sensitive to inadvertent saturation of reactant sites, as T_1 will not restore their polarization, and hence this artifact will be cumulative throughout the ST experiments. To control for this oversensitivity to inadvertent Gluc depolarization, we normalized the Lac signal observed during the ST pulsing by the Lac signal observed after the intermediate's pulsing is stopped, which will be concomitantly reduced in the event of Gluc depolarization.

The high temporal resolution of hyperpolarized NMR metabolic measurements enabled the non-invasive determination of the initial glycolytic rates reported in this study. These results can be compared with previous studies of Gluc metabolism, including kinetic measurements on the metabolism in T47D cells carried out non-invasively by thermal ^{13}C NMR with a temporal resolution of approximately 20 min (29). The K_m value arising from these thermal equilibrium experiments was similar (2.3 ± 1.0 mM) to that observed in our studies (3.5 ± 1.5 mM). The V_{max} of Lac production obtained (34 ± 4 fmol/cell/min) is in reasonable accord with rates of Gluc consumption observed in earlier thermal NMR studies, assuming a Gluc → 2Lac process (12.6 ± 1.2 fmol/cell/min); it is, however, approximately twice that reported for Lac synthesis (15.8 ± 0.9 fmol/cell/min). This discrepancy may reflect the fact that, although dissolution DNP measures initial rates of Lac production, 'slower' experiments also factor in the subsequent conversion of Lac to other metabolic products, resulting in an apparent reduction in the former's production rate.

The concentrations of intracellular intermediates observed here are of the same magnitude as those observed previously in MCF-7 breast cancer (36) and colon cancer (37) cells. In those studies, low-concentration intermediates were detected in cell extracts, where the living state of the cells was quenched. The rapid turnover rates of all enzymatic processes – as seen by the present work – emphasize the importance of measuring such metabolites in living systems. The ability to measure the time delay between turning off intermediate pulsing and complete recovery of the Lac signal also gives unprecedented temporal sensitivity to metabolic processes in living systems, of the kind heretofore achieved only *ex vivo* (38). By probing metabolic rate information, the DNP NMR 'clock' may find the answers to diverse important biological questions, including the reversibility of enzymatic reactions and metabolic compartmentalization. Further investigations of this kind may also shed light on our assumption of negligible reverse rates for the hyperpolarized markers along the glycolytic pathway.

Since Otto Warburg noted the increased rates of glycolysis in cancer nearly a century ago (1), there has been much speculation as to why cancer would switch from oxidative phosphorylation to energetically inefficient glycolysis (39,40). In recent years, a new hypothesis has emerged, suggesting that cancers favor increased rates of glycolysis as many of the ensuing intermediates can be diverted to produce the array of small molecules necessary for rapid cell proliferation (41–43). This theory suggests that, not only the glycolytic flux, but also the concentration and kinetics of the intermediate metabolites, are important features of the cancer metabolic phenotype. The unprecedented ability afforded by *ex situ* DNP, in combination with

ST methods of the kind discussed here, shows great promise for the measurement of glycolytic intermediates in living cells. Using perdeuterated ^{13}C-enriched Gluc as a biomarker, we have shown that the dissolution DNP setting can detect not only the rate of Lac production, but also several other glycolytic intermediates that could act as practical biomarkers of cancer glycolysis. In effect, several studies have shown that, in tumors, the concentrations of glycolytic intermediates as measured *ex vivo*, change in response to therapeutic treatments (44,45). If further applied *in vivo*, this could provide important additional information in the diagnosis and treatment of cancer. Moreover, following Gluc's fate by hyperpolarized shift-resolved spectroscopic imaging may have advantages over ^{18}F-fluorodeoxyglucose positron emission tomography. As Gluc is metabolically active, such a form of imaging will report on the fate of a metabolic process that is actually active under *in vivo* natural conditions. This could also be relevant for research in other areas involving high physiological Gluc uptake, including areas of inflammation and functional studies in the brain. Work in progress includes the use of the perfusion–injection system with gradients to better quantify 'invisible' intermediates and to characterize changes in response to environment or therapeutic treatments, and the application of hyperpolarized U-^{13}C,^{2}H$_7$-Gluc to animal cancer models to characterize the efficacy of Lac's production for the detection of cancer.

Acknowledgements

This research was supported by the Israel Science Foundation (ISF 447/09), EU'S FP7 Metaflux Grant # 264780, DIP Project 710907 (Ministry of Education and Research, Germany), a Helen and Kimmel Award for Innovative Investigation and the generosity of the Perlman Family Foundation. T.H. gratefully acknowledges a fellowship from the Clore Foundation (Israel). H.D. is the incumbent of the Fred and Andrea Fallek Professorial Chair for Breast Cancer Research.

REFERENCES

1. Warburg O, Posener K, Negelein E. The metabolism of cancer. Biochem. Zeitschr. 1924; 152: 129–169.
2. Chen Z, Lu W, Garcia-Prieto C, Huang P. The Warburg effect and its cancer therapeutic implications. J. Bioenerg. Biomembr. 2007; 39: 267–274.
3. Moreno-Sanchez R, Rodrıguez-Enrıquez S, Marın-Hernandez A, Saavedra E. Energy metabolism in tumor cells. FEBS 2007; 274: 1393–1418.
4. Cairns RA, Harris IS, Mak TW. Regulation of cancer cell metabolism. Nat. Rev. Cancer 2011; 11: 85–95.
5. Tennant DA, Duran R, Gottlieb E. Targeting metabolic transformation for cancer therapy. Nat. Rev. Cancer 2010; 10: 267–277.
6. Kelloff GJ, Hoffman JM, Johnson B, Scher HI, Siegel BA, Cheng EY, Cheson BD, O'Shaughnessy J, Guyton KZ, Mankoff DA, Shankar L, Larson SM, Sigman CC, Schilsky RL, Sullivan DC. Progress and promise of FDG-PET imaging for cancer patient management and oncologic drug development. Clin. Cancer Res. 2005; 11: 2785–2808.
7. Pinilla I, Rodriguez-Vigil B, Gomez-Leon N. Integrated ^{18}FDG PET/CT: utility and applications in clinical oncology. Clin. Med. 2008; 2: 181–198.
8. Glunde K, Artemov D, Penet MF, Jacobs MA, Bhujwalla ZM. Magnetic resonance spectroscopy in metabolic and molecular imaging and diagnosis of cancer. Chem. Rev. 2010; 110: 3043–3059.
9. Glunde K, Jiang L, Moestue SA, Gribbestad IS. MRS and MRSI guidance in molecular medicine: targeting and monitoring of choline and glucose metabolism in cancer. NMR Biomed. 2011; 24: 673–690.
10. London R. ^{13}C labeling in studies of metabolic regulation. Prog. Nucl. Magn. Reson. Spectrosc. 1988; 20: 337–383.
11. Rivenzon-Segal D, Boldin-Adamsky S, Seger D, Seger R, Degani H. Glycolysis and glucose transporter 1 as markers of response to hormonal therapy in breast cancer. Int. J. Cancer 2003; 107: 177–182.
12. Wijnen JP, Van der Graaf M, Scheenen TW, Klomp DW, de Galan BE, Idema AJ, Heerschap A. In vivo ^{13}C magnetic resonance spectroscopy of a human brain tumor after application of ^{13}C-1-enriched glucose. Magn. Reson. Imaging 2010; 28: 690–697.
13. Moreno-Sánchez R, Saavedra E, Rodríguez-Enríquez S, Gallardo-Pérez JC, Quezada H, Westerhoff HV. Metabolic control analysis indicates a change of strategy in the treatment of cancer. Mitochondrion 2010; 10: 626–639.
14. Yang C, Richardson A, Osterman A, Smith J. Comparative metabolomics of breast cancer. Metabolomics 2008; 4: 13–29.
15. Klawitter J, Anderson N, Klawitter J, Christians U, Leibfritz D, Eckhardt SG, Serkova NJ. Time-dependent effects of imatinib in human leukaemia cells: a kinetic NMR-profiling study. Br. J. Cancer 2009; 100: 923–931.
16. Fan TW, Lane AN, Higashi RM, Yan J. Stable isotope resolved metabolomics of lung cancer in a SCID mouse model. Metabolomics 2011; 7: 257–269.
17. Forbes NS, Meadows AL, Clark DS, Blanch HW. Estradiol stimulates the biosynthetic pathways of breast cancer cells: detection by metabolic flux analysis. Metab. Eng. 2006; 8: 639–652.
18. Cuperlovic-Culf M, Barnett DA, Culf AS, Chute I. Cell culture metabolomics: applications and future directions. Drug Discov. Today 2010; 15: 610–621.
19. Mashego MR, Wu L, Van Dam JC, Ras C, Vinke JL, Van Winden WA, Van Gulik WM, Heijnen JJ. MIRACLE: mass isotopomer ratio analysis of U-^{13}C-labeled extracts. A new method for accurate quantification of changes in concentrations of intracellular metabolites. Biotechnol. Bioeng. 2004; 85: 620–628.
20. Ardenkjær-Larsen JH, Fridlund B, Gram A, Hansson G, Hansson L, Lerche MH, Servin R, Thaning M, Golman K. Increase in signal-to-noise ratio of >10,000 times in liquid-state NMR. Proc. Natl. Acad. Sci. U. S. A. 2003; 100: 10 158–10 163.
21. Abragam A, Goldman M. Principles of dynamic nuclear polarization. Rep. Prog. Phys. 1978; 41: 395–467.
22. Day SE, Kettunen MI, Gallagher FA, Hu DE, Lerche M, Wolber J, Golman K, Ardenkjaer-Larsen JH, Brindle KM. Detecting tumor response to treatment using hyperpolarized ^{13}C magnetic resonance imaging and spectroscopy. Nat. Med. 2007; 13: 1382–1387.
23. Harris T, Eliyahu G, Frydman L, Degani H. Kinetics of hyperpolarized ^{13}C$_1$-pyruvate transport and metabolism in living human breast cancer cells. Proc. Natl. Acad. Sci. U. S. A. 2009; 106: 18 131–18 136.
24. Merritt ME, Harrison C, Storey C, Jeffrey FM, Sherry AD, Malloy CR. Hyperpolarized ^{13}C allows a direct measure of flux through a single enzyme-catalyzed step by NMR. Proc. Natl. Acad. Sci. U. S. A. 2007; 104: 19 773–19 777.
25. Keshari KR, Wilson DM, Chen AP, Bok R, Larson PE, Hu S, Van Criekinge M, Macdonald JM, Vigneron DB, Kurhanewicz J. Hyperpolarized [2-^{13}C]-fructose: a hemiketal DNP substrate for in vivo metabolic imaging. J. Am. Chem. Soc. 2009; 131: 17 591–17 596.
26. Gallagher FA, Kettunen MI, Day SE, Hu DE, Ardenkjaer-Larsen JH, Zandt R, Jensen PR, Karlsson M, Golman K, Lerche MH, Brinkdle KM. Magnetic resonance imaging of pH in vivo using hyperpolarized ^{13}C-labelled bicarbonate. Nature 2008; 453: 940–943.
27. Chen AP, Kurhanewicz J, Bok R, Xu D, Joun D, Zhang V, Nelson SJ, Hurd RE, Vigneron DB. Feasibility of using hyperpolarized [1-^{13}C]lactate as a substrate for in vivo metabolic ^{13}C MRSI studies. Magn. Reson. Imaging 2008; 26: 721–726.
28. Kadkhodaei M, Wu H, Brant DA. Conformational dynamics of the (1➔4)- and (1➔6)-linked α-D-glucans using ^{13}C-NMR relaxation. Biopolymers 1991; 31: 1581–1592.
29. Rivenzon-Segal D, Rushkin E, Polak-Charcon S, Degani H. Glucose transporters and transport kinetics in retinoic acid-differentiated T47D human breast cancer cells. Am. J. Physiol. Endocrinol. Metab. 2000; 279 (3): E508–E519.
30. Curzon EH, Hawkes GE, Randall EW, Britton HG, Fazakerley GV. Conformational analysis of 2- and 3-phosphoglyceric acids by ^{1}H and ^{13}C nuclear magnetic resonance spectroscopy. J. Chem. Soc. Perkin Trans. 2 1981; 3: 494–499.
31. Massiot D, Fayon F, Capron M, King I, Le Calve S, Alonso B, Durand JO, Bujoli B, Gan ZH, Hoatson G. Modelling one- and two-dimensional solid-state NMR spectra. Magn. Reson. Chem. 2002; 40: 70–76.
32. Forsen S, Hoffman RA. Study of moderately rapid chemical exchange reactions by means of nuclear magnetic double resonance. J. Chem. Phys. 1963; 39: 2892–2901.

33. Meier S, Karlsson M, Jensen PR, Lerche MH, Duus JO. Metabolic pathway visualization in living yeast by DNP-NMR. Mol. Biosyst. 2011; 7: 2834–2836.
34. Meier S, Jensen PR, Duss JØ. Real-time detection of central carbon metabolism in living *Escherichia coli* and its response to perturbations. FEBS Lett. 2011; 585: 3133–3138.
35. Meier S, Jensen PR, Duss JØ. Direct observation of metabolic differences in living *Escherichia coli* strains K-12 and BL21. ChemBioChem. 2011; 13: 308–310.
36. Hugo F, Mazurek S, Zander U, Eigenbrodt E. In vitro effect of extracellular AMP on MCF-7 breast cancer cells: inhibition of glycolysis and cell proliferation. J. Cell. Physiol. 1992; 153: 539–549.
37. Thangaraju M, Carswell KN, Prasad PD, Ganapathy V. Colon cancer cells maintain low levels of pyruvate to avoid cell death caused by inhibition of HDAC1/HDAC3. Biochem. J. 2009; 417: 379–389.
38. Noh K, Gronke K, Luo B, Takors R, Oldiges M, Wiechert W. Metabolic flux analysis at ultra short time scale: isotopically non-stationary ^{13}C labeling experiments. J. Biotechnol. 2007; 129: 249–267.
39. Gatenby RA, Gillies RJ. Why do cancers have high aerobic glycolysis? Nat. Rev. Cancer 2004; 4: 891–899.
40. Kim JW, Dang CV. Cancer's molecular sweet tooth and the Warburg effect. Cancer Res. 2006; 66: 8927–8930.
41. DeBerardinis RJ, Lum JJ, Hatzivassiliou G, Thompson CB. Brick by brick: metabolism and tumor cell growth. Cell Metab. 2008; 7: 11–20.
42. Vander Heiden MG, Cantley LC, Thompson CB. Understanding the Warburg effect: the metabolic requirements of cell proliferation. Science 2009; 324: 1029–1033.
43. Lunt SY, Vander Heiden MG. Aerobic glycolysis: meeting the metabolic requirements of cell proliferation. Annu. Rev. Cell Dev. Biol. 2011; 27: 441–464.
44. Hirayama A, Kami K, Sugimoto M, Sugawara M, Toki N, Onozuka H, Kinoshita T, Saito N, Ochiai A, Tomita M, Esumi H, Soga T. Quantitative metabolome profiling of colon and stomach cancer microenvironment by capillary electrophoresis time-of-flight mass spectrometry. Cancer Res. 2009; 69: 4918–4925.
45. Muruganandham M, Alfieri AA, Matei C, Chen Y, Sukenick G, Schemainda I, Hasmann M, Saltz LB, Koutcher JA. Metabolic signatures associated with a NAD synthesis inhibitor – induced tumor apoptosis identified by ^{1}H-decoupled-^{31}P magnetic resonance spectroscopy. Clin. Cancer Res. 2005; 11: 3503–3513.

APPENDIX A: EXTRACTION OF METABOLIC RATES FROM SELECTIVELY PULSED HYPERPOLARIZED EXPERIMENTS

For a Gluc $\xrightarrow{v}$ Lac kinetic process generating Lac at a rate $v_{Lac} = 2 \cdot k_{Gluc} \cdot [Gluc]$, the corresponding M_Z magnetizations of these two species can be written as follows (if we assume that the concentration of Gluc does not change during the experiment):

$$\frac{dM_{Z,Gluc}(t)}{dt} = \frac{d\left(P_{Gluc}(t)\cdot[Gluc]_0\right)}{dt} = -\frac{1}{T_{1,Gluc}}\cdot P_{Gluc}(t)\cdot[Gluc]_0 \qquad (A1a)$$

$$\frac{dM_{Z,Lac}(t)}{dt} = v_{Lac}\cdot P_{Gluc}(t) - \frac{1}{T_{1,Lac}}\cdot dM_{Z,Lac}(t) \qquad (A1b)$$

where $P_{Gluc}(t)$ is the Gluc polarization as a function of time and $[Gluc]_0$ is the initial concentration. Solving these equations for the magnetization of the two species yields:

$$M_{Z,Gluc}(t) = [Gluc]_0\cdot P_{Gluc}(0)\cdot e^{-\frac{t}{T_{1,Gluc}}} \qquad (A1c)$$

$$M_{Z,Lac}(t) = v_{Lac}\cdot P_{Gluc}(0)\cdot\left(\frac{e^{-\frac{t}{T_{1,Lac}}} - e^{-\frac{t}{T_{1,Gluc}}}}{\frac{1}{T_{1,Gluc}} - \frac{1}{T_{1,Lac}}}\right). \qquad (A1d)$$

If we define $\Delta\rho = \frac{1}{T_{1,Gluc}} - \frac{1}{T_{1,Lac}}$, the Z-magnetization Lac can be simplified to:

$$M_{Z,Lac}(t) = v_{Lac}\cdot P_{Gluc}(0)\cdot e^{-\frac{t}{T_{1,Gluc}}}\cdot\left(\frac{e^{\Delta\rho\cdot t} - 1}{\Delta\rho}\right) \qquad (A1e)$$

On application of a polychromatic pulse at time t that imparts a 90° nutation to Lac's magnetization and a small tip angle α to the Gluc spins, the signal S observed for each compound will be given by:

$$S_{Gluc}(t) = c\cdot\sin\alpha_{Gluc}\cdot[Gluc]_0\cdot P_{Gluc}(0)\cdot e^{-\frac{t}{T_{1,Gluc}}} \qquad (A2a)$$

$$S_{Lac}(t) = c\cdot v_{Lac}\cdot P_{Gluc}(0)\cdot e^{-\frac{t}{T_{1,Gluc}}}\cdot\left(\frac{e^{\Delta\rho\cdot t} - 1}{\Delta\rho}\right) \qquad (A2b)$$

where c is a spectrometer-dependent constant. The polychromatic pulses eliciting these signals will be applied at constant repetition time TR; therefore, every time that signals are observed at times $t = n\cdot TR$ ($n = 1,2,\ldots$), the Lac magnetization will return to zero, whereas Gluc's magnetization will remain relatively unaffected. This implies that the Lac signal measured at time t will also depend on TR as:

$$S_{Lac}(t,TR) = c\cdot v_{Lac}\cdot P_{Gluc}(0)\cdot e^{-\frac{t}{T_{1,Gluc}}}\cdot\left(\frac{e^{\Delta\rho\cdot TR} - 1}{\Delta\rho}\right) \qquad (A.2c)$$

which is Equation [3]. The uncertain variables c and $P_{Gluc}(0)$ can be avoided by normalizing the Lac signal by the Gluc signal at every time point t:

$$R_{Lac}(TR) = \frac{S_{Lac}(t,TR)}{S_{Gluc}(t)} = \frac{v_{Lac}}{\sin\alpha_{Gluc}\cdot[Gluc]_0}\cdot\left(\frac{e^{\Delta\rho\cdot TR} - 1}{\Delta\rho}\right) \qquad (A.3a)$$

which is Equation [4]. In the case that $\Delta\rho\cdot TR << 1$, this equation can be further simplified:

$$R_{Lac}(TR) = \frac{S_{Lac}(t,TR)}{S_{Gluc}(t)} = \frac{v_{Lac}\cdot TR}{\sin\alpha_{Gluc}\cdot[Gluc]_0} \qquad (A.3b)$$

APPENDIX B: QUANTIFICATION OF INTERMEDIATES BY PULSED SATURATION TRANSFER IN HYPERPOLARIZED NMR

To model the effects of saturating an intermediate's magnetization and observing its consequences on a Lac signal originating from hyperpolarized Gluc, we simplify the model in APPENDIX A by adding two assumptions: (i) that $T_{1,Gluc} = T_{1,Int} = T_{1,Lac} = T_1$, i.e. that all carbonyls relax in the cells at approximately the same rates; and (ii) that the rate of the reverse processes in hyperpolarized-detected experiments is negligible and hence $v_{Lac} = f\cdot k_{Int}\cdot[Int]_{SS}$, where the factor $f = 1$ for three-carbon intermediates and $f = 2$ for six-carbon intermediates to account for the conversion of a six-carbon precursor into two identical three-carbon products, and $[Int]_{SS}$ is the intermediate's steady-state concentration. With these assumptions, the magnetization of an intermediate involved in glycolysis metabolism can be modeled as:

$$\frac{dM_{Z,Int}(t)}{dt} = k_{Int}\cdot[Int]_{SS}\cdot P_{Gluc}(t) - k_{Int}\cdot M_{Z,Int}(t) - \frac{1}{T_1}\cdot M_{Z,Int}(t) \quad \text{(B.1a)}$$

Solving this equation yields an intermediate's Z-magnetization:

$$M_{Z,Int}(t) = [Int]_{SS}\cdot P_{Gluc}(0)\cdot e^{-\frac{t}{T_1}}\cdot\left(1 - e^{-k_{Int}\cdot t}\right) \quad \text{(B.1b)}$$

The variables $[Int]_{SS}$ and k_{Int} are interrelated, and the above equation can also be written as:

$$M_{Z,Int}(t) = [Int]_{SS}\cdot P_{Gluc}(0)\cdot e^{-\frac{t}{T_1}}\cdot\left(1 - e^{-\frac{v_{Lac}}{f\cdot[Int]_{SS}}\cdot t}\right) \quad \text{(B.1c)}$$

In the case of a polychromatic pulse that applies a 90° nutation on the intermediate and a low flip angle α nutation on Gluc every TR, the intermediate signal will thus be:

$$S_{Int}(t, TR) = c\cdot[Int]_{SS}\cdot P_{Gluc}(0)\cdot e^{-\frac{t}{T_1}}\cdot\left(1 - e^{-\frac{v_{Lac}}{f\cdot[Int]_{SS}}\cdot TR}\right) \quad \text{(B2)}$$

On normalization by the Gluc signal at every time point, this intermediate signal ratio becomes:

$$R_{Int}(TR) = \frac{[Int]_{SS}}{\sin\alpha_{Gluc}\cdot[Gluc]_0}\cdot\left(1 - e^{-\frac{v_{Lac}}{f\cdot[Int]_{SS}}\cdot TR}\right) \quad \text{(B3)}$$

which is Equation [6].

Pulsing on an intermediate's signal will also affect the observed Lac magnetization, and therefore its observable signal. This leads to the saturation transfer effects described in the article, which can be modeled as:

$$\frac{dM_{Z,Lac}(t)}{dt} = v_{Lac}\cdot\left(\frac{1}{f}\right)\cdot P_{Int}(t) + v_{Lac}\cdot\left(1 - \frac{1}{f}\right)\cdot P_{Gluc}(t) - \frac{1}{T_1}\cdot M_{Z,Lac}(t) \quad \text{(B.4a)}$$

Solving this equation yields:

$$M_{Z,Lac}(t) = v_{Lac}\cdot P_{Gluc}(0)\cdot t\cdot e^{-\frac{t}{T_1}} - [Int]_{SS}\cdot P_{Gluc}(0)\cdot e^{-\frac{t}{T_1}}\cdot\left(1 - e^{-\frac{v_{Lac}}{f\cdot[Int]_{SS}}\cdot t}\right) \quad \text{(B4b)}$$

Applying now a polychromatic pulse that imparts a 90° nutation on both the intermediate (to saturate it) and on Lac (to detect the effects of the saturation), and a low flip angle α nutation on Gluc at time t, leads to a Lac signal:

$$S_{Lac}(t) = c\cdot v_{Lac}\cdot P_{Gluc}(0)\cdot t\cdot e^{-\frac{t}{T_1}} - [Int]_{SS}\cdot P_{Gluc}(0)\cdot e^{-\frac{t}{T_1}}\cdot\left(1 - e^{-\frac{v_{Lac}}{f\cdot[Int]_{SS}}\cdot t}\right) \quad \text{(B5)}$$

Normalizing this by the Gluc signal at every time point yields the ratio:

$$R_{Lac}(TR) = \frac{v_{Lac}\cdot TR}{\sin\alpha_{Gluc}[Gluc]_0} - \frac{[Int]_{SS}}{\sin\alpha_{Gluc}[Gluc]_0}\cdot\left(1 - e^{-\frac{v_{Lac}}{f\cdot[Int]_{SS}}\cdot TR}\right) \quad \text{(B6)}$$

which is Equation [6].

A valuable additional degree of freedom in these saturation transfer-type experiments arises by choosing different recycling delays to saturate the putative intermediate peak (TR_{Int}) from those used to measure the observable Lac peaks (TR_{Lac}). In this case, the intermediate's polarization is no longer a continuous function. It can be shown, however, that the observed Lac signal will be given by:

$$S_{Lac}(t, TR_{Lac}, , TR_{Int}) = c\cdot v_{Lac}\cdot P_{Gluc}(0)\cdot TR_{Lac}\cdot e^{-\frac{t}{T_1}} - \frac{TR_{Lac}}{TR_{Int}}\cdot[Int]_{SS}\cdot P_{Gluc}(0)\cdot e^{-\frac{t}{T_1}}\cdot\left(1 - e^{-\frac{v_{Lac}}{f\cdot[Int]_{SS}}\cdot TR_{Int}}\right) \quad \text{(B7)}$$

which simplifies to Equation [B5] in the case $TR_{Int} = TR_{Lac}$. Dividing this signal by the Gluc peak observed at TR_{Lac} yields the ratio:

$$R_{Lac}(TR_{Lac}, , TR_{Int}) = \frac{v_{Lac}\cdot TR_{Lac}}{\sin\alpha_{Gluc}[Gluc]_0} - \frac{TR_{Lac}}{TR_{Int}}\cdot\frac{[Int]_{SS}}{\sin\alpha_{Gluc}[Gluc]_0}\cdot\left(1 - e^{-\frac{v_{Lac}}{f\cdot[Int]_{SS}}\cdot TR_{Int}}\right) \quad \text{(B8)}$$

which corresponds to Equation [7]. To decrease errors arising from the comparison of different experiments, we define a ratio Q between the Gluc-normalized Lac signal in the presence and absence of intermediate pulsing, which will only depend on TR_{Int}:

$$Q_{Lac}(TR_{Int}) = 1 - \frac{[Int]_{SS}}{TR_{Int}\cdot v_{Lac}}\cdot\left(1 - e^{-\frac{v_{Lac}}{f\cdot[Int]_{SS}}\cdot TR_{Int}}\right) \quad \text{(B9)}$$